KINEMATIC ANALYSIS AND PERFORMANCE EVALUATION OF 6R INSTRUMENTED SPATIAL LINKAGES

Gianluca Gatti, Domenico Mundo, Guido Danieli
Department of Mechanical Engineering, University of Calabria, 87036 Arcavacata di Rende (CS), Italy
E-mail: g.gatti@unical.it

Received June 2009, Accepted November 2009
No. 09-CSME-31, E.I.C. Accession 3117

ABSTRACT

Six-degree-of-freedom instrumented spatial linkages are often used to measure anatomical joint motion for clinical studies or research applications in biomechanics. Their appropriate design is a fundamental issue to allow for accurate measurements and ease of application, and this mainly relies on addressing the kinematic analysis of the linkage. The aim of this paper is to integrate and extend past literature in the field by giving a generalized set of guidelines and ready-to-use mathematical relationships to approach the whole kinematic analysis of a general instrumented spatial linkage in a systematic way. The direct kinematics is formulated using common robotics formulation and, with reference to a specific linkage architecture, a geometrical approach is proposed to solve for the inverse kinematics in closed-form. Kinematic error analysis is addressed in a generalized way by using differential transformation theory, and it is then applied to the specific case under study. By the proper definition of a virtual joint, the inverse kinematics is used to estimate the static performance of the linkage over its specific task space.

ANALYSE CINÉMATIQUE ET ÉVALUATION DE LA PERFORMANCE D'UN MÉCANISME SPATIAL INSTRUMENTÉ 6R

RÉSUMÉ

Des mécanismes spatiaux instrumentés à six degrés de liberté sont souvent utilisés en biomécanique pour mesurer les mouvements anatomiques des articulations. L'adéquation de leur conception est le point fondamental qui permet l'exactitude et la facilité des mouvements, et cela dépend principalement de l'analyse cinématique des articulations. Le but de notre recherche est d'intégrer et de faire progresser les connaissances dans le domaine, en donnant un ensemble de lignes directrices générales, et de relations mathématiques générales pour faire l'analyse cinématique globale d'un mécanisme spatial instrumenté de façon systématique. La cinématique directe est exprimée en utilisant la formulation robotique courante et, en référence à une architecture d'articulation spécifique, une approche géométrique est proposée pour la résolution cinématique inverse en boucle fermée. On s'intéresse à l'analyse d'erreur cinématique de façon générale en utilisant la théorie de la transformation différentielle, et elle ensuite appliquée au cas spécifique étudié. Par une définition adéquate d'un joint virtuel, la cinématique inverse est utilisée pour estimer la performance statique de l'articulation dans l'espace de travail spécifique.

1. INTRODUCTION

In biomechanical applications, instrumented spatial linkages (ISLs) are some of the most commonly used measuring devices for anatomical joints motion measurement. They usually consist of a series of rigid links connected to each other by rotational transducers. In order to measure the complete six degree-of-freedom (DOF) motion of anatomical joints [1, 2], six-revolute instrumented spatial linkages (6R-ISLs) are used, where the end fixtures are attached to the two bones of the joint of interest, thereby allowing motion to be estimated from the linkage geometry and transducer readings.

The first application of 6R-ISL to anatomical joint motion seems to be reported in 1972 by Kinzel et al. [3], who presented the analytical basis for such a measuring system and described its application to the study of the shoulder kinematics of a dog. He also gave some advances in the mechanical design of such measuring devices in [4]. The use of ISLs to measure three-dimensional articular joints motion is reported, for instance, with application to the human elbow joint [5] and the human knee [6]. A comprehensive set of guidelines for the design of 6R-ISLs was given by Kirstukas et al. [7], who proposed a combined empirical-quantitative technique based on computer graphics and numerical methods as aid in developing 6R-ISL for different anatomical joints and demonstrated its effectiveness for knee-joint measurements. This latter work seems to be the last attempt in proposing a methodology to characterize and compare different ISLs.

Subsequent researches seem, in fact, to be mainly related to the application of commercially available or specifically designed ISLs for research purposes or clinical investigations, either for in-vitro [8–11] or in-vivo [12–15] measurement of joint dynamic motion. Gardner et al. [16] applied an ISL to accurately measure the relative motion at a bony fracture and, recently, Nordquist and Hull [17] designed an ISL to get a better understanding of the extent of dynamic motion of joints during sporting activities.

This paper is focused on the kinematic analysis and performance evaluation of ISLs, which are critical issues for their design and for comparative studies. Although the importance of kinematic analysis was mentioned in [7], useful considerations were given and critical issues pointed out, the objective of that work was mainly to address the design phase in a descriptive manner. By illustrating how to approach the kinematic analysis of general ISLs in a quantitative and systematic way, the main contribution of the present paper is twofold: (i) to propose a geometrical approach to solve for the inverse kinematics in closed-form, and (ii) to perform a detailed error analysis based on a general differential transformation theory. With reference to a specific in-house manufactured ISL for knee-joint measurement – which is described beforehand in the following section – a set of comprehensive and ready-to-use set of guidelines are thus reported, which guide the reader through the main steps involved in the analysis, and a procedure to evaluate the ISL theoretical resolution is illustrated by the adoption of a virtual joint to define the operating task space.

2. INSTRUMENT DESCRIPTION

The mechanical linkage described in this work is specifically designed for knee-joint applications; a virtual model of the system is illustrated in Fig. 1a, while Fig. 1b shows a photograph of the final instrument, assembled on an artificial leg system. Links are made of aluminium and directly connected by revolute optical encoders (IVO GmbH & Co. KG, model GA241) with a resolution of about 7.7×10^{-4} rad per step. This linkage is used to estimate the pose of its distal link (assumed to be rigidly connected with the tibia) relative to the proximal

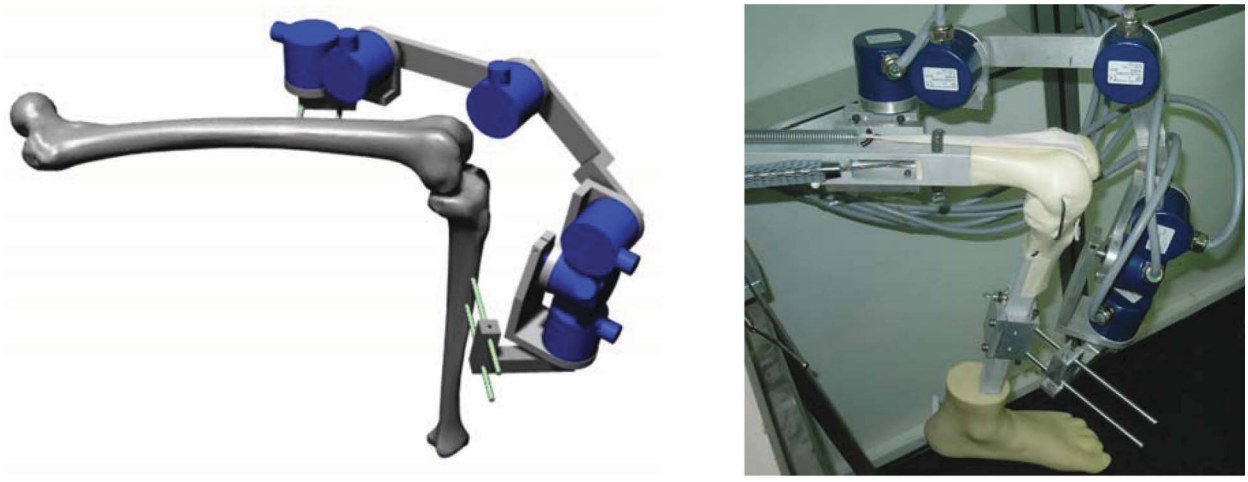

(a) (b)

Fig. 1. The actual 6R-ISL. (a) Virtual representation (CAD models of tibia and femur were created by Marco Viceconti and are available on the Internet through the BEL Repository managed by the Instituti Ortopedici Rizzoli, Bologna, Italy). (b) Picture of the real system on a workshop leg system (MITA Endo Leg, Medical Models Ltd. UK).

(assumed to be rigidly connected with the femur), so as to detect the envelope of joint motions as the leg is bent or extended.

Although knee-joint kinematics is a complex interaction between bones, ligaments, cartilage and muscles, and may only be completely described by six degrees of motion during dynamic activities [1, 2], the main components of this motion are commonly described in terms of flexion-extension and longitudinal internal-external rotation of the tibia with respect to the femur. The ISL is thus designed so as to accommodate as much as possible for those two motion components separately, allowing for a proper measurement. By then following the basic guidelines reported in [7], an 'elbow-type' structure is selected, which – as firstly demonstrated in [18] – assures a maximization of the work volume of the linkage. The specific arrangement of the revolute joints in the ISL assures that the configuration assumed by all of them except the last is constrained to a planar movement, which roughly identifies the plane in which the knee movement may be supposed to develop. In this plane, the algebraic sum of the second, third and fourth joint angles would give an estimate of the knee flexion angle, while the sixth would provide a very rough measure of the longitudinal rotation. The kinematic solution of the ISL shown in Fig. 1 differs from that described in [7], where the last three joint axes intersect to allow for an easy solution of the inverse kinematics.

3. KINEMATIC MODELLING

The kinematic model relates the joint angles of the linkage to the relative location of its extreme fixtures, and it is a function of the linkage geometry. According to robotics terminology, the proximal segment of the linkage will be referred to as the *base* (fixed to the femur), while the distal segment will be referred to as the *end-effector* (fixed to the tibia).

Given a 6R-ISL, the kinematic model thus relates the 6-length vector of joint coordinates $\mathbf{q} = [q_1, \cdots, q_6]^T$ to the pose (position and orientation) of the end-effector, which may be given as a 4-by-4 transformation matrix of the following form [19]

$$\mathbf{T} = \begin{bmatrix} \mathbf{R} & \mathbf{P} \\ 0 & 1 \end{bmatrix}, \tag{1}$$

where **R** is a 3-by-3 rotational matrix and **P** is a 3-by-1 position vector.

The kinematic model is a function of a set of geometrical parameters, e.g. the D-H parameters [20], which may be generally grouped into an r-length kinematic parameters vector $\mathbf{k} = [k_1, \cdots, k_r]^T$, defining the shape and geometry of the structure. Direct kinematics $F(\cdot)$ and inverse kinematics $G(\cdot)$ are then defined as

$$\mathbf{T} = F(\mathbf{q}, \mathbf{k}), \tag{2}$$

$$\mathbf{q} = G(\mathbf{T}, \mathbf{k}). \tag{3}$$

The direct kinematics $F(\cdot)$ is used to estimate the relative position and orientation between the distal and proximal fixtures as a function of the joint angles, while the inverse kinematics $G(\cdot)$, which solves for the joint angles given the relative pose of the end fixtures, is used in simulations, kinematic analysis and for evaluating theoretical performances. For the purposes of this paper, nominal kinematics is considered.

4. DIRECT KINEMATICS

In order to measure knee motion from transducer readings, a direct kinematics is implemented and the kinematic description of the linkage is addressed by following a link-to-link transformation matrix approach, which is commonly used in robotics [20].

An orthogonal right-handed reference frame is attached to each link of the mechanical system and the relative pose between two reference frames, say $\{i\}$ and $\{j\}$, is given by a 4-by-4 transformation matrix $\mathbf{T}_j^i$ defining the pose of frames $\{i\}$ relative to frame $\{j\}$ – where, according to Eq. (1), **R** is a 3-by-3 rotational matrix which contains, as columns, the components of the unit-vectors of the axes of frame $\{j\}$ expressed in frame $\{i\}$, and **P** is a 3-by-1 vector defining the position of the origin of frame $\{j\}$ relative to frame $\{i\}$.

4.1. Frame Assignment

The first step to kinematic modelling is thus to assign a proper coordinate frame to each link. For a 6-DOF open-loop kinematic chain, joints and moving linkages are numbered from 1 to 6 starting from the base, which is referred to as link 0. A coordinate system $\{i\text{-}1\}$, for $i = 1, \cdots, 6$ is then attached to the corresponding i-1 link. These coordinate systems are orthogonal and their axes obey the right-hand rule. According to the standard D-H convention as described in [20], the assignment of each reference frame consists of assigning (a) the z-axis, (b) the origin and (c) the x-axis, as explained below (the remaining y-axis direction is chosen according to the right-hand rule):

(a) The z-axis of frame $\{i\text{-}1\}$ is chosen along the axis of joint i.
(b) The origin of the frame $\{i\text{-}1\}$ is placed at the intersection of joint axis i and the common perpendicular between joint axis i and i-1, while the origin of frame $\{0\}$ may be chosen arbitrarily along joint axis 1.
(c) The x-axis of reference frame $\{i\text{-}1\}$ is chosen coincident to the common perpendicular direction between joint axes i and i-1, while for frame $\{0\}$ is chosen arbitrarily.

Reference frame {6}, referred to as the end-effector frame, may be chosen arbitrarily.

A schematic view of the 6R-ISL kinematics with its embedded frames – in its reference configuration – is shown in Fig. 2, where the particular location of reference frame {6} is also indicated.

4.2. Kinematic Equation

The equation for the direct kinematics of the ISL is obtained by consecutive homogeneous transformation matrices from the base frame to the end-effector frame, as

$$\mathbf{T}_6^0 = \prod_{i=1}^{6} \mathbf{T}_i^{i-1}, \tag{4}$$

where $\mathbf{T}_i^{i-1}$ is the transformation matrix from frame {i-1} to frame {i}, and it is given – provided that frame assignment is performed according to the steps indicated in Section 4.1 – as the following concatenation of four homogeneous transformation matrices

$$\mathbf{T}_i^{i-1} = Rot(z, q_i + \theta_i) \cdot Trans(z, d_i) \cdot Trans(x, a_i) \cdot Rot(x, \alpha_i),$$

which are functions of four D-H parameters, namely θ_I, d_i, a_i, α_i, and where the following 4-by-4

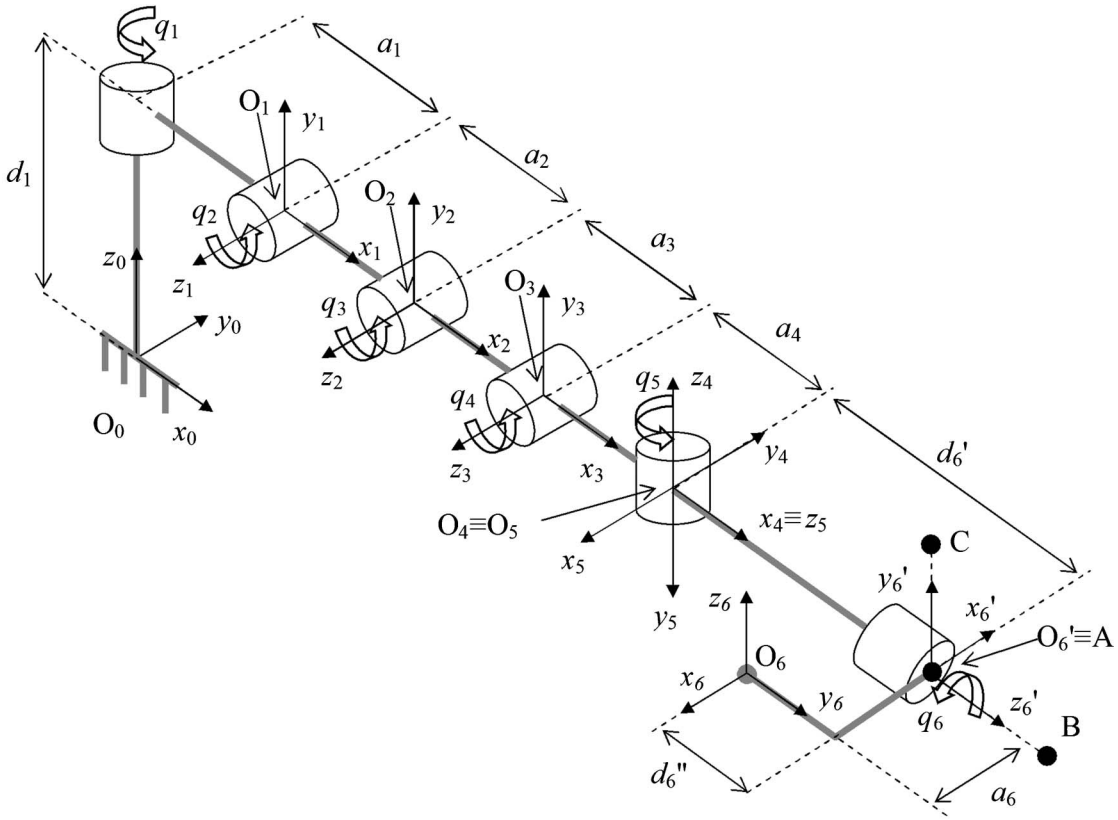

Fig. 2. Schematic view of the actual 6R-ISL with embedded frames and nominal geometrical parameters, in its reference configuration. Parameters $d_6' = 100$mm and $d_6'' = -75$ mm, to give $d_6 = d_6' + d_6''$, are used into the text. Points A, B and C are used to solve for the inverse kinematics.

elementary transformation matrices are defined

$$Trans(x,\cdot)=\begin{bmatrix}1&0&0&\cdot\\0&1&0&0\\0&0&1&0\\0&0&0&1\end{bmatrix},\ Trans(y,\cdot)=\begin{bmatrix}1&0&0&0\\0&1&0&\cdot\\0&0&1&0\\0&0&0&1\end{bmatrix},\ Trans(z,\cdot)=\begin{bmatrix}1&0&0&0\\0&1&0&0\\0&0&1&\cdot\\0&0&0&1\end{bmatrix},$$

$$Rot(x,\cdot)=\begin{bmatrix}1&0&0&0\\0&\cos(\cdot)&-\sin(\cdot)&0\\0&\sin(\cdot)&\cos(\cdot)&0\\0&0&0&1\end{bmatrix},\ Rot(y,\cdot)=\begin{bmatrix}\cos(\cdot)&0&\sin(\cdot)&0\\0&1&0&0\\-\sin(\cdot)&0&\cos(\cdot)&0\\0&0&0&1\end{bmatrix},$$

$$Rot(z,\cdot)=\begin{bmatrix}\cos(\cdot)&-\sin(\cdot)&0&0\\\sin(\cdot)&\cos(\cdot)&0&0\\0&0&1&0\\0&0&0&1\end{bmatrix}.$$

The four D-H parameters are determined as the arguments of the corresponding elementary transformations that make frame $\{i\text{-}1\}$ be superimposed to frame $\{i\}$.

Equation (4) thus defines the direct kinematics of the ISL, according to the formulation of Eq. (2). For the actual ISL, D-H parameters used to model its geometry are given in Table 1.

For a joint coordinates vector $\mathbf{q}=[0,0,0,0,0,0]^T$ and nominal kinematics, the ISL assumes the configuration shown in Fig. 2, i.e. the reference configuration.

5. INVERSE KINEMATICS

The solution to the inverse kinematics of ISLs may be addressed by one of the two main and well-established approaches which are reported in the literature: the analytical-algebraic approach and the numerical approach. The algebraic approach is proposed to derive closed-form solutions for the joint variables. The basic idea of this approach, which is described for instance in [21–25], is to transform the kinematic equations into high order polynomials in some trigonometric function of the joint variables, and then determine all of the roots by using a root solver. Most recent researches about this approach have been focused on the description of

Table 1. Nominal values for the D-H parameters used to model the actual ISL.

i	θ_i(rad)	d_i(mm)	a_i(mm)	α_i(rad)
1	0	66	60	$\pi/2$
2	0	0	160	0
3	0	0	160	0
4	0	0	60	$-\pi/2$
5	$-\pi/2$	0	0	$-\pi/2$
6	0	25	50	$\pi/2$

singular configurations [26] or on some related computational issues [27]. This method is suitable for non-redundant articulated architectures, and in particular for 'elbow-type' ISLs with the last three joint axes intersecting – i.e. the so-called Pieper's solution [19] – which is also the case of most ISL architectures, as for example those used in [7, 17].

Most numerical algorithms are based on the multidimensional Newton-Raphson method or similar techniques [28–30]. Although numerical methods are much less efficient than analytical methods, they could be conveniently adopted for ISL applications, where the solution to the inverse kinematics is used for off-line purposes.

In this section, an alternative analytical technique is proposed, which uses vector geometry as an intuitive approach to solve for the inverse kinematics in closed-form, i.e. to solve for the joint angles $\mathbf{q}$ analytically, given the nominal geometry of the linkage and the end-effector pose. The approach is based on the determination of the absolute position of point $O_{i\text{-}1}$ ($i=1,\cdots,6$), which identifies the origin of frame $\{i\text{-}1\}$ according to the D-H convention. In fact, once expressions of the coordinates of those points are determined in frame $\{0\}$, each joint angle q_i ($i=1,\cdots,6$) may be found as the angle between known vectors.

It is noted that the approach cannot be generalized as a whole, since it depends on the particular configuration of joints in the ISL, and reference will be thus made to the actual system. However, some guidelines and suggestions are given to address the problem for different ISL architectures.

To identify the end-effector pose geometrically, three points A, B and C may be conveniently defined in frame $\{6\}$, and, for the actual case, they are labelled as black circles in Fig. 2. The absolute position of those three points defines the ISL end-effector pose in a unique way and may be determined from the $\mathbf{T}_6^0$ matrix as

$$\begin{cases} {}^0A = \mathbf{T}_6^0 \cdot {}^6A \\ {}^0B = \mathbf{T}_6^0 \cdot {}^6B, \\ {}^0C = \mathbf{T}_6^0 \cdot {}^6C \end{cases}$$

where the superscripts on the left-hand side identify the frames with respect to which point coordinates are given. So far, the approach may be generalized, while here below follows a step-by-step description of the problem solution, which applies to the actual particular geometry.

Defining the auxiliary frame $\{6'\}$, as sketched in Fig. 2, points A and B are conveniently chosen to be aligned to the z_6' axis, while point C is chosen to be along the y_6' axis. Their relative coordinates are given below as

$$\begin{cases} {}^{6'}A = \{\,0 \quad 0 \quad 0\,\}^T \\ {}^{6'}B = \{\,0 \quad 0 \quad 1\,\}^T \\ {}^{6'}C = \{\,0 \quad 1 \quad 0\,\}^T \end{cases}, \quad \begin{cases} {}^{6}A = \{\,-50 \quad 75 \quad 0\,\}^T \\ {}^{6}B = \{\,-50 \quad 76 \quad 0\,\}^T \\ {}^{6}C = \{\,-50 \quad 75 \quad 1\,\}^T \end{cases}.$$

It is then noted that, due to the particular arrangement of revolute joints in the actual system, all points $O_{i\text{-}1}$ ($i=1,\cdots,6$) are constrained to move on a plane Γ, which is defined as the plane passing through the z_0 axis and inclined by q_1 from the x_0z_0 plane. This latter joint angle is thus determined as

$$q_1 = \arctan\left(\frac{{}^0O_5(y)}{{}^0O_5(x)}\right) \text{ or } q_1 = \pi + \arctan\left(\frac{{}^0O_5(y)}{{}^0O_5(x)}\right)$$

where ${}^0O_5 \equiv {}^0O_4 = {}^0O_6' - {}^0\vec{u}_{AB} \cdot d_6'$, and the following relations hold: ${}^0O_6' \equiv {}^0A$, ${}^0\vec{u}_{AB} = \dfrac{{}^0B - {}^0A}{\|{}^0B - {}^0A\|}$. It is noted how the equation for q_1 introduces a first double solution in the inverse kinematics.

Joint angles q_5 and q_6 are determined as the angles between the following vectors

$$q_5 = \text{angle}\left(\overline{O_3O_4}, \overline{O_5O_6}'\right),$$

$$q_6 = \text{angle}\left(\vec{n}, \overline{AC}\right),$$

where $\vec{n}$, which is a vector orthogonal to plane x_4y_4, and O_3 are determined as follows, by introducing an auxiliary coordinate system x_4', z_4'. This is laying on plane Γ and is defined such as $z_4' \| z_0$ and $O_4' \equiv O_4$, as sketched in Fig. 3a. This figure also illustrates how O_3 may assume two different locations, introducing a second double solution in the inverse kinematics. If R_3 and Z_3 indicate the coordinates of point O_3 in this auxiliary coordinate system, the following relations hold

$$\begin{aligned} {}^0O_3 &= {}^0O_4 + \{\, R_3\cos(q_1) \quad R_3\sin(q_1) \quad Z_3 \,\}^T \\ {}^0\vec{n} &= \{\, Z_3\cos(q_1) \quad Z_3\sin(q_1) \quad -R_3 \,\}^T \end{aligned} \quad . \tag{5a, b}$$

By then imposing the geometric constraints

$$\begin{aligned} \left\|\overline{O_3O_4}\right\| &= a_4 \\ \overline{O_5O_{6'}} \cdot \vec{n} &= 0 \end{aligned},$$

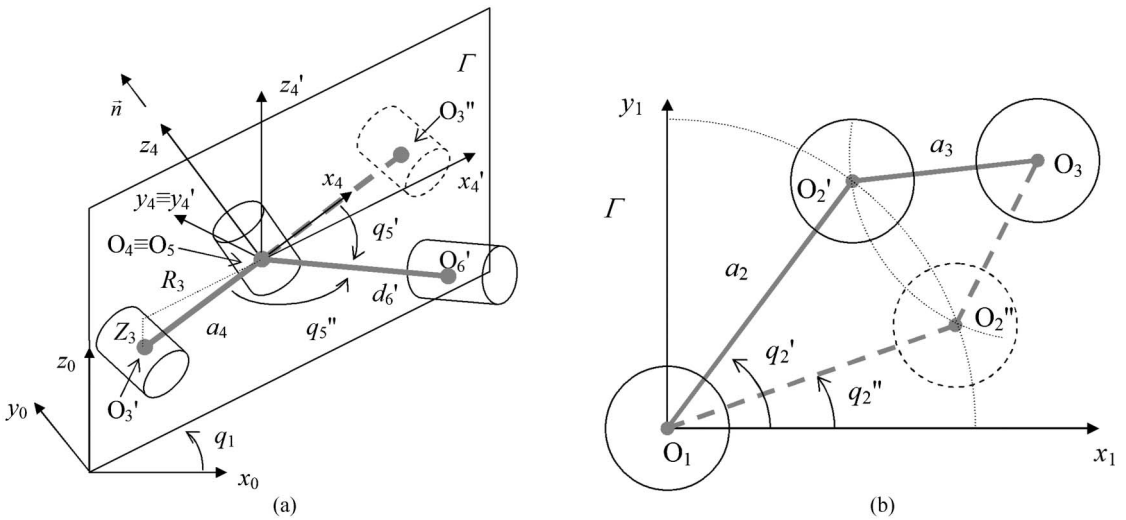

Fig. 3. Schematic representation of multiple solutions in solving inverse kinematics. (a) Relative location of joint 4, 5 and 6. Once the locations of O_5 and O_6' are determined based on the end-effector pose, two possible locations for O_3 are identified, namely O_3' and O_3''. This results in a double solution in terms of q_5. (b) Relative location (in plane Γ) of joint 2, 3 and 4. Once the locations of O_1 and O_3 are determined, two possible locations for O_2 are identified, namely O_2' and O_2''. This results in a double solution in terms of q_2.

which may be rewritten, by using Eqs. (5a,b), in the following algebraic form

$$\begin{aligned} & {R_3}^2 + {Z_3}^2 = {a_4}^2 \\ & \left({}^0O_6(x) - {}^0O_5(x)\right) Z_3 \cos(q_1) + \left({}^0O_6(y) - {}^0O_5(y)\right) Z_3 \sin(q_1) + , \\ & \quad + \left({}^0O_6(z) - {}^0O_5(z)\right)(-R_3) = 0 \end{aligned} \tag{6a, b}$$

a solution is obtained in terms of R_3 and Z_3, as

$$\begin{aligned} R_3 &= \frac{\pm a_4}{\sqrt{1 + \left(\frac{\left({}^0O_6(z) - {}^0O_5(z)\right)}{({}^0O_6(x) - {}^0O_5(x))\cos(q_1) + ({}^0O_6(y) - {}^0O_5(y))\sin(q_1)} \right)^2}} \\ Z_3 &= \frac{R_3\left({}^0O_6(z) - {}^0O_5(z)\right)}{({}^0O_6(x) - {}^0O_5(x))\cos(q_1) + ({}^0O_6(y) - {}^0O_5(y))\sin(q_1)} \end{aligned} \tag{7a, b}$$

In the case where the denominators in Eqs. (7a,b) go to zero, then the solution is given as

$$\begin{aligned} R_3 &= 0 \\ Z_3 &= \pm a_4 \end{aligned} , \tag{8a, b}$$

while, if either denominator or numerator in Eq. (7b) go to zero, there is an indetermination in the fifth joint angle, which can be either equal to $\pm\pi/2$.

Substituting Eqs. (7a,b) or Eqs. (8a,b) back into Eq. (5a) the two possible solutions for point O_3 are identified.

Joint angles q_2, q_3 and q_4 depend on the location of point O_2 according to the following relationships

$$q_2 = \text{angle}\left(\{ \cos(q_1) \quad \sin(q_1) \quad 0 \}^T, \overline{O_1O_2} \right),$$

$$q_3 = \text{angle}\left(\overline{O_1O_2}, \overline{O_2O_3} \right),$$

$$q_4 = \text{angle}\left(\overline{O_2O_3}, \overline{O_3O_4} \right),$$

where the location of point O_1 is obtained as ${}^0O_1 = \{ a_1 \cos(q_1) \quad a_1 \sin(q_1) \quad d_1 \}^T$.

To solve for O_2 – which, again, may assume two different locations according to what is sketched in Fig. 3b, thus introducing a third double solution in the inverse kinematics – R_2 and Z_2 are introduced as its coordinates along the x_1 and y_1 axes, respectively. Its absolute coordinates in frame {0} are then written as

$${}^0O_2 = {}^0O_1 + \{ R_2\cos(q_1) \quad R_2\sin(q_1) \quad Z_2 \}^T,$$

which may be substituted into the following geometric constraints

$$\begin{array}{l} \left\|\overline{O_1O_2}\right\| = a_2 \\ \overline{O_2O_3} = a_3 \end{array},$$

to obtain

$$\begin{array}{l} {R_2}^2 + {Z_2}^2 = {a_2}^2 \\ \left(R_2 - R^{*2}\right)^2 + \left(Z_2 - Z^{*2}\right)^2 = {a_3}^2 \end{array}. \qquad (9a, b)$$

Equations (9a,b) may be solved to get

$$\begin{array}{l} Z_2 = \pm \dfrac{-2GZ^* \pm \sqrt{(-2GZ^*)^2 - 4({a_3}^2 + {a_2}^2)\left(G^2 - {L_2}^2 R^{*}2\right)}}{2({a_3}^2 + {a_2}^2)} \\ R_2 = \dfrac{G - Z_2 Z^*}{R^*} \end{array}, \qquad (10a, b)$$

where the following auxiliary variables are defined

$$\begin{array}{l} R^* = O_3(x)\cos(q_1) - O_1(x)\cos(q_1) \\ Z^* = O_3(z) - O_1(z) \\ 2G = R^*2 + Z^{*2} - {a_3}^2 + {a_2}^2 \end{array}.$$

In the case where R^* is equal to zero, the set of Eqs. (10a,b) is replaced by

$$\begin{array}{l} Z_2 = \frac{G}{Z^*} \\ R_2 = \pm\sqrt{{L_2}^2 - {Z_2}^2} \end{array}.$$

It is finally noted how the ambiguity in the location of some points $O_{i\text{-}1}$, $(i = 1, \cdots, 6)$, as described above, results in the fact that, given the pose of the end-effector frame, a set of multiple joint angle solutions does exist.

6. KINEMATIC ERROR ANALYSIS

The kinematic performance of an ISL is usually estimated in terms of its theoretical resolution, which is defined as the smallest incremental movement the system end-effector is capable of sensing. Resolution is affected by the ISL geometry and the individual joint transducers resolution, and it thus depends on the instantaneous linkage configuration. It represents an ideal performance, which means that, in a given workspace, the actual measured instrument accuracy will never be smaller than its computed resolution. Although the effect of joint clearances [31, 32] and link compliances [33] in serial kinematic chains has been also investigated, those are considered negligible for most of ISL design architectures.

In a preliminary design phase, when a rough estimate of the instrument resolution, i.e. its order of magnitude, may help in selecting the proper geometry and the appropriate transducers, simple expressions may be adopted, which are given below, for the linear and angular components of the end-effector endpoint error, respectively, as

$$\begin{aligned} RS_{l,\max} &\approx \sum_{i=1}^{6} h_i(\mathbf{q})\delta q_i \\ RS_{a,\max} &\approx \sum_{i=1}^{6} \delta q_i \end{aligned}, \tag{11a, b}$$

where δq_i is the ith transducer resolution and h_i is the distance between the end-effector endpoint and the revolute axis of the ith joint. Such expressions simply consider that all joints are aligned with each other, and thus represent the upper limits for the highest possible errors that are expected: actual values will always be smaller than these. Eq. (11a) may easily be evaluated based on the nominal geometry and for the fully-extended linkage configuration, where all distances h_i are expected to give the highest contribution to the overall error.

Resolution may also be evaluated more accurately in a specified portion of the workspace (often referred to as task space), provided that the direct and inverse kinematics of the ISL are known. More rigorous expressions to estimate the instrument resolution may also be computed as discussed in [34] for some specific ISL arrangements. A different approach was also recently proposed by Briot and Bonev [35] for a parallel architecture. In any case, it is of interest to estimate the linear and angular resolution using a single intuitive number, even within a given task space of different possible ISL configurations.

Differential transformation theory [36] is applied here to obtain an estimate of the linear differential change from the ideal pose of the ISL end-effector frame to its actual pose, due to joint uncertainties. In fact, this latter pose may be given, by borrowing Eq. (4), as

$${}^{actual}\mathbf{T}_6^0 = \prod_{i=1}^{6} {}^{actual}\mathbf{T}_i^{i-1}, \tag{12}$$

where the superscript '*actual*' on the upper left-hand side of each transformation matrix indicates the actual expression, as affected by transducers resolution. Each of the transformation matrices in Eq. (12) may be written as the sum of its nominal expression plus a linear differential error as

$${}^{actual}\mathbf{T}_i^{i-1} = \mathbf{T}_i^{i-1} \pm \delta\mathbf{T}_i^{i-1},$$

where the error $\delta\mathbf{T}_i^{i-1}$ is due to a small variation in the corresponding joint variable, and may be given as

$$\delta\mathbf{T}_i^{i-1} = \frac{\partial\mathbf{T}_i^{i-1}}{\partial q_i}\delta q_i.$$

Since all joints in a 6R-ISL are revolute, the following relations hold

$$\frac{\partial \mathbf{T}_i^{i-1}}{\partial q_i} = \frac{\partial Rot(z, q_i + \theta_i)}{\partial q_i} \cdot Rot(z, q_i + \theta_i)^{-1} \cdot \mathbf{T}_i^{i-1} = \mathbf{D} \cdot \mathbf{T}_i^{i-1},$$

$$\mathbf{D} = \frac{\partial Rot(z, q_i + \theta_i)}{\partial q_i} \cdot Rot(z, q_i + \theta_i)^{-1} = \begin{bmatrix} 0 & -1 & 0 & 0 \\ 1 & 0 & 0 & 0 \\ 0 & 0 & 0 & 0 \\ 0 & 0 & 0 & 0 \end{bmatrix},$$

and the actual pose of the end-effector relative to the absolute reference frame, given by Eq. (12), may be rewritten as

$${}^{actual}\mathbf{T}_6^0 = \prod_{i=1}^{6} (\mathbf{I} \pm \delta q_i \mathbf{D}) \cdot \mathbf{T}_i^{i-1}.$$

The end-effector pose error is finally defined as the change from its nominal error-free pose to the actual one, namely

$$\delta \mathbf{T}_6^0 = \left(\mathbf{T}_6^0\right)^{-1} \cdot {}^{actual}\mathbf{T}_6^0. \tag{13}$$

From the pose error, given by Eq. (13) as a 4-by-4 homogeneous transformation matrix, a linear and an angular error, as single scalar numbers, may be determined as follows.

The linear error is indeed defined by the position error vector norm, namely

$$\delta l = \sqrt{\left(\delta \mathbf{T}_6^0(1,4)\right)^2 + \left(\delta \mathbf{T}_6^0(2,4)\right)^2 + \left(\delta \mathbf{T}_6^0(3,4)\right)^2}. \tag{14}$$

The angular error is determined using the *equivalent angle-axis* representation of a finite rotational matrix, as described in [19]. Given two frames and thus the relative orientation between them in terms of an orthogonal rotational matrix **R** – which may be extracted from the 4-by-4 homogeneous transformation matrix as illustrated in Eq. (1) – it is always possible to determine an axis around which one reference frame may be rigidly rotated to be superimposed to the other. The angle that describes such a rotation (and the corresponding axis) may be used to define the difference in orientation between those two poses. The formula for such an angle determination is reported below as

$$\delta \phi = \arccos\left(\frac{\delta \mathbf{T}_6^0(1,1) + \delta \mathbf{T}_6^0(2,2) + \delta \mathbf{T}_6^0(3,3) - 1}{2}\right). \tag{15}$$

In order to define a consistent set of end-effector configurations − which are representative for the specific ISL application and which may be used to define a proper task space within which to estimate resolution − the following two-steps criterion is conveniently adopted: *Step-1*, a simple kinematic model of the anatomical joint under investigation is implemented; *Step-2*,

assuming the ISL attached to such virtual joint, its inverse kinematics is solved for a set of m end-effector poses that are obtained by 'moving' the virtual joint within an appropriate range of motion. Within such a generated task space, the maximum values of the errors as given by Eq. (14) and Eq. (15) may be considered as the resolution of the ISL. This is given in terms of linear and angular components as

$$RS_l = \max(L),\ RS_a = \max(\Phi), \tag{16a, b}$$

where $L = \left[\delta l_1, \cdots, \delta l_j, \cdots, \delta l_m\right]$ and $\Phi = \left[\delta\phi_1, \cdots, \delta\phi_j, \cdots, \delta\phi_m\right]$.

6.1. Computational Application and Numerical Validation

As a computational example, the theoretical formulation described above is applied to the actual ISL architecture, for which the fully-extended configuration is sketched in Fig. 2. In this situation, expressions for distances h_i in Eq. (11a), are given below as

$$\begin{aligned} h_1 &= \sqrt{(a_1 + a_2 + a_3 + a_4 + d_6)^2 + {a_6}^2} \\ h_2 &= a_2 + a_3 + a_4 + d_6 \\ h_3 &= a_3 + a_4 + d_6 \\ h_4 &= a_4 + d_6 \\ h_5 &= \sqrt{{d_6}^2 + {a_6}^2} \\ h_6 &= a_6 \end{aligned} \quad ,$$

and, for the encoder resolution given in Section 2, the linear and angular components of the end-effector endpoint error computed by using the upper-bound estimates from Eq. (11a) and Eq. (11b), respectively, give the following values; $RS_{l,\max} \approx 1.004$ mm and $RS_{a,\max} \approx 0.0046$ rad.

A simulation is then implemented, by applying the differential transformation theory, as presented above, to estimate the ISL resolution in a given operating task space. This is dependent on the particular application of the actual ISL, i.e. anatomical knee joint measurements. In this case, for *Step-1*, a simple 2-DOF mathematical model of the knee-joint, as sketched in Fig. 4, is defined by means of the following transformation matrix equation

$$\begin{aligned} {}^{knee}\mathbf{T}_6^0 = {} & Trans(y, -r_1) \cdot Trans(x, r_2) \cdot Rot(y, \alpha) \cdot \\ & \cdot Trans(x, r_3) \cdot Rot(x, r_4 + \beta) \cdot Trans(z, r_5) \cdot Rot(z, -\pi/2) \end{aligned}, \tag{17}$$

where $r_1, \cdots, r_5$ are geometric parameters defining the dimensions of the 'leg' of the model, and α, β are the two degrees of freedom relative to the flexion-extension and internal-external rotation, respectively, which let the model be 'moved'. For *Step-2,* the inverse kinematics of the ISL, as reported in Section 5, is solved for a set of $m = 150$ end-effector poses defined by a ${}^{knee}\mathbf{T}_6^0$, as in Eq. (17), where $r_1 = 60$ mm, $r_2 = 160$ mm, $r_3 = 160$ mm, $r_4 = \pi/6$ rad $r_5 = 60$ mm, and angles α, β are randomly varied in the range 0° – 130° (flexion) and $\pm 30^\circ$ (longitudinal rotation), respectively. *Step-2* is repeated 10 times, and for each trial the linear and angular resolutions computed from Eqs. (16a,b) are shown in Fig. 5a and Fig. 5b, respectively.

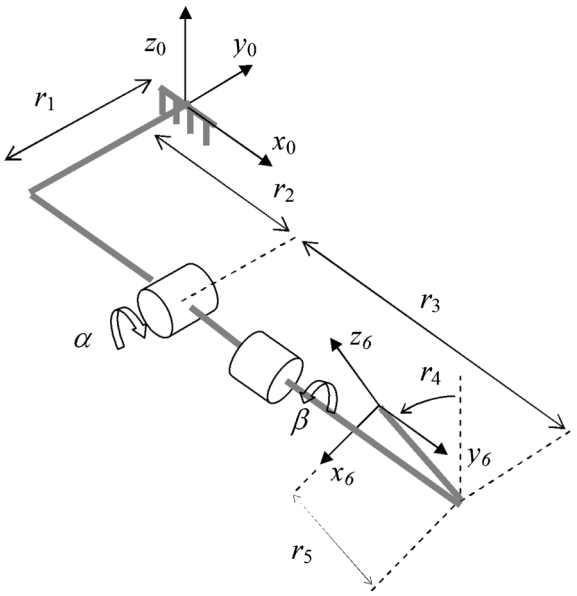

Fig. 4. Schematic representation of the 'virtual joint', i.e. the 2-DOF model of the knee articulation, used to estimate ISL kinematic performance. Geometric parameters $r_1, \ldots, r_5$ (whose values are given into the text) are used to define the 'leg', while angles α, β represent the two degrees of freedom relative to the flexion-extension and longitudinal internal-external rotation, respectively.

To validate such estimates for the resolution of the actual ISL, a second numerical simulation is performed. In this case, for each of the previous 10 trials a random error (within the joint resolution) is added to each joint variable for every jth configuration ($j = 1, \cdots, m$), thus simulating uncertainty in the transducer readings. The change in terms of nominal and corrupted end-effector pose is computed using Eq. (13), and corresponding linear error $\delta\tilde{l}_j$ and

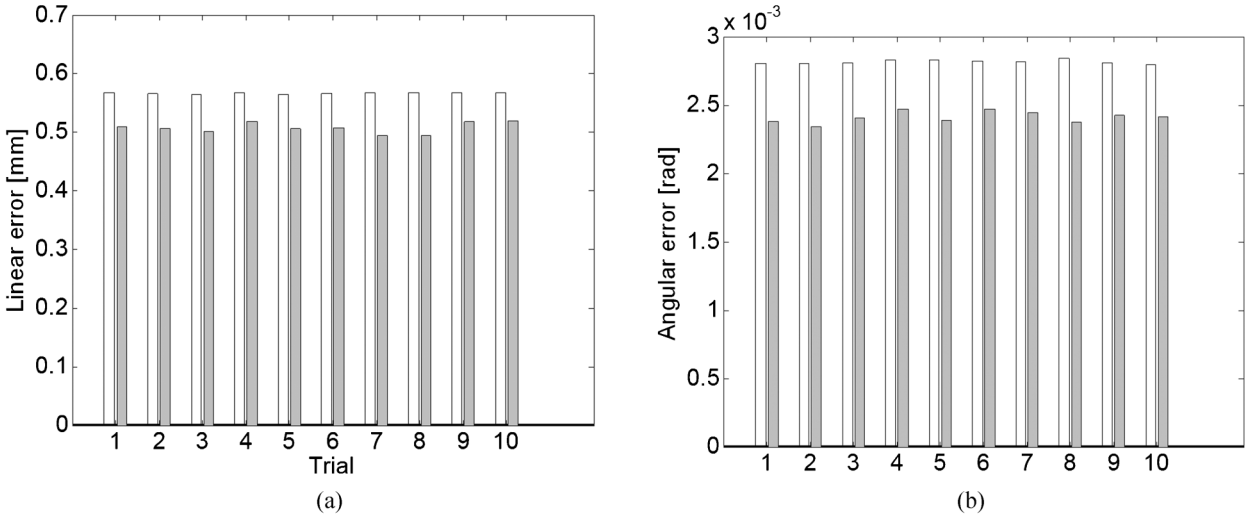

Fig. 5. Comparison, for 10 different trials, between the resolution of the actual ISL computed by applying differential transformation theory, Eqs. (16,b), (white bars), and the end-effector pose error computed numerically by adding randomly distributed uncertainties to the joint variables, Eqs. (18a,b), (grey bars). (a) Linear error and (b) angular error.

angular error $\delta\tilde{\phi}_j$ $(j=1,\cdots,m)$ are computed using Eqs. (14) and (15), respectively. For each of the 10 trials, two error distributions, $\tilde{L}=\left[\delta\tilde{l}_1,\ \cdots,\delta\tilde{l}_j,\ \cdots,\delta\tilde{l}_m\right]$ and $\tilde{\Phi}=\left[\delta\tilde{\phi}_1,\ \cdots,\delta\tilde{\phi}_j,\ \cdots,\delta\tilde{\phi}_m\right]$, are then evaluated, and linear and angular end-effector errors are estimated and given as single numbers to capture 99.7% confidence interval as

$$E_l=\mu_{\tilde{L}}+3\sigma_{\tilde{L}},\ E_a=\mu_{\tilde{\Phi}}+3\sigma_{\tilde{\Phi}}, \tag{18a, b}$$

where μ and σ stand for mean and standard deviation, respectively.

Results of this second numerical simulation are also shown in Fig. 5 and compared to the results of the first simulation. It is evident how the resolution computed by applying the differential transformation theory, i.e. Eqs. (16a,b), is always slightly greater than the end-effector pose error obtained numerically by adding random errors to each joint variable, i.e. Eqs. (18a,b). Such a comparison validates the proposed approach, in fact since differential transformation theory only considers the upper bounds for encoders uncertainty, it leads to a corresponding upper bound for the end-effector pose error, i.e. the ISL resolution by definition. Experimental performance and results after calibration [34] also validate such estimated theoretical predictions.

7. CONCLUSIONS

With an application to a particular 6R-ISL, this paper gives detailed and ready-to-use guidelines for the complete kinematic analysis of such linkages, with the aim to integrate and extend the methodology suggested in [7] for correct ISL design. The actual ISL is, in fact, designed, by following the general guidelines reported by Kirstukas et al. in [7], as an 'elbow-type' structure, which makes it particularly suitable to measure human knee-joint articulation motion, for which the instrument is specifically designed. By applying all the mathematical considerations to the actual case as an example, the formulation of the direct kinematics is reported from literature and, in particular: (i) a geometrical approach is proposed to solve for the inverse kinematics of general ISLs in closed-form, and (ii) a detailed error analysis is performed using a general differential transformation theory.

The inverse kinematics is solved analytically by using a geometrical approach, which is based on the determination of the origins of the reference frames identifying each link in the mechanism. Although the proposed technique is case-dependent, suggestions and useful considerations are given to approach the inverse kinematics solution for different ISL architectures. Usually, as pointed out in the text, the appropriate configuration of joints and geometry may offer the possibility to define a series of geometrical relationships/constraints and to derive all solutions in closed form.

A detailed error analysis is performed using differential transformation theory, and general expressions are given for estimating the ISL resolution within the operating task space, which is dependent on the particular application. A virtual joint model is used to define the poses of the end-effector in such specific volume via the inverse kinematics. To validate the proposed methodology, numerical simulations are performed on the actual ISL and compared to the predicted estimates.

REFERENCES

1. Kinzel, G.L. and Gutkowski, L.J., "Joint models, degrees of freedom, and anatomical motion measurement," *ASME Journal of Biomechanical Engineering*, Vol. 105, pp. 55–62, 1983.

2. Bull, A.M.J. and Amis, A.A., ''Knee-joint motion: description and measurement,'' *Proceedings of the Institution of Mechanical Engineers Part H Journal of Engineering in Medicine*, Vol. 212, pp. 357–372, 1998.
3. Kinzel, G.L., Hall, Jr A.S. and Hillberry, B.M., ''Measurement of the total motion between two body segments. I. Analytical development,'' *Journal of Biomechanics*, Vol. 5, No. 1, pp. 93–105, 1972.
4. Kinzel, G.L., ''On the design of instrumented linkages for the measurement of relative motion between two rigid bodies,'' *Ph.D dissertation*, Purdue University, Lafayette, Ind., 1973.
5. Chao, E.Y.S., An, K.N., Askew, L.J. and Morrey, B.F., ''Electrogoniometer for the measurement of human elbow joint rotation,'' *ASME Journal of Biomechanical Engineering*, Vol. 102, pp. 301–310, 1980.
6. Grood, E.S. and Suntay, W.J., ''A joint coordinate system for the clinical description of three-dimensional motions: application to the knee,'' *ASME Journal of Biomechanical Engineering*, Vol. 105, pp. 136–144, 1983.
7. Kirstukas, S.J., Lewis, J.L. and Erdman A.G., ''6R instrumented spatial linkages for anatomical joint motion measurement-part 1: design,'' *ASME Journal of Biomechanical Engineering*, Vol. 114, No. 1, pp. 92–100, 1992.
8. Noyes, F.R., Grood, E.S., Cummings, J.F. and Wroble, R.R., ''An analysis of the pivot shift phenomenon,'' *American Journal of Sports and Medicine*, Vol. 19, pp. 148–155, 1991.
9. Sorger, J.I., Federle, D., Kirk, P.G., Grood, E., Cochran, J. and Levy, M., ''The posterior cruciate ligament in total knee arthroplasty,'' *Journal of Arthroplasty*, Vol. 12, No. 8, pp. 869–879, 1997.
10. Lewandowski, P.J., Askew, M.J., Lin, D.F., Hurst, F.W. and Melby, A., ''Kinematics of posterior cruciate ligament-retaining and -sacrificing mobile bearing total knee arthroplasties: An in vitro comparison of the New Jersey LCS meniscal bearing and rotating platform prostheses,'' *Journal of Arthroplasty*, Vol. 12, No. 7, pp. 777–784, 1997.
11. Jan, S.V.S., Salvia, P., Hilal, I., Sholukha, V., Rooze, M. and Clapworthy, G., ''Registration of 6-DOFs electrogoniometry and CT medical imaging for 3D joint modelling,'' *Journal of Biomechanics*, Vol. 35, pp. 1475–1484, 2002.
12. Townsend, M.A., Izak, M. and Jackson, R.W., ''Total motion knee goniometry,'' *Journal of Biomechanics*, Vol. 10, pp. 183–193, 2002.
13. Shiavi, R., Limbird, T., Frazer, M. and Stivers, K., ''Strauss A and Abramovitz J. Helical motion analysis of the knee. II. Kinematics of uninjured and injured knees during walking and pivoting,'' *Journal of Biomechanics*, Vol. 20, pp. 653–665, 1987.
14. Shiavi, R., Limbird, T., Frazer, M., Stivers, K., Strauss, A. and Abramovitz, J., ''Helical motion analysis of the knee. I. Methodology for studying kinematics during locomotion,'' *Journal of Biomechanics*, Vol. 20, pp. 459–469, 1987.
15. Salvia, P., Woestyn, L., David, J.H., Feipel, V., Jan, S.V.S., Klein, P. and Rooze, M., ''Analysis of helical axes, pivot and envelope in active wrist circumduction,'' *Clinical Biomechanics*, Vol. 15, pp. 103–111, 2000.
16. Gardner, T.N., Evans, M. and Kyberd, P.J., ''An instrumented spatial linkage for monitoring relative three-dimensional motion between fracture fragments,'' *ASME Journal of Biomechanical Engineering*,'' Vol. 118, No. 4, pp. 586–594, 1996.
17. Nordquist, J. and Hull, M.L., ''Design and Demonstration of a New Instrumented Spatial Linkage for Use in a Dynamic Environment: Application to Measurement of Ankle Rotations During Snowboarding,'' ASM*E Journal of Biomechanical Engineering*, Vol. 129, pp. 231–239, 2007.
18. Paden, B. and Sastry, S., ''Optimal kinematic design of 6R manipulators,'' *International Journal of Robotics Research*, Vol. 7, No. 3, pp. 43–61, 1988.

19. Craig, J.J., *Introduction to Robotics Mechanics and Control*, Addison-Wesley, New York, 1989.
20. Mooring, B.W., Roth, Z. and Driels, M.R., *Fundamentals of manipulator calibration*, John Wiley & Sons, New York,1991.
21. Duffy, J. and Crane, C., "A displacement analysis of the general spatial 7-link, 7R mechanism," *Mechanism and Machine Theory*, Vol. 15, No. 3, pp. 153–169, 1980.
22. Lee, H.Y. and Liang, C.G., "Displacement analysis of the general spatial 7-link, 7R mechanism," *Mechanism and Machine Theory*, Vol. 23, No. 3, pp. 219–226, 1988.
23. Wampler, C. and Morgan, A., "Solving the 6R inverse position problem using a generic-case solution methodology," *Mechanism and Machine Theory*, Vol. 26, No. 1, pp. 91–106, 1991.
24. Raghavan, M. and Roth, B., "Inverse kinematics of the general 6R manipulator and related linkages," *ASME Journal of Mechanical Design*, Vol. 115, No. 3, pp. 502–508, 1993.
25. Lee, H.Y. and Reinholtz, C.F., "Inverse kinematics of serial-chain manipulators," *ASME Journal of Mechanical Design*, Vol. 118, No. 3, pp. 396–404, 1996.
26. Hayes, M.J.D, Husty, M.L. and Zsombor-Murray, P.J., "Singular configurations of wrist-partitioned 6R serial robots: A geometric perspective for users," *Transactions of the Canadian Society for Mechanical Engineering*, Vol. 26, No. 1, pp. 41–45, 2002.
27. Husty, M.L., Pfurner, M. and Schrocker, H.P., "A new and efficient algorithm for the inverse kinematics of a general serial 6R manipulator," *Mechanism and Machine Theory*, Vol. 42, No. 1, pp. 66–81, 2007.
28. Cheng, H. and Gupta, K.C., "A study of robot inverse kinematics based upon the solution of differential-equations," *Journal of Robotic Systems*, Vol. 8, No. 2, pp. 159–175, 1991.
29. Chen, I.M., Yang, G.L. and Kang, I.G. "Numerical inverse kinematics for modular reconfigurable robots," *Journal of Robotic Systems*, Vol. 16, No. 4, pp. 213–225, 1999.
30. Zhao, Y.J., Huang, T. and Yang, Z.Y., "A new numerical algorithm for the inverse position analysis of all serial manipulators," *Robotica*, Vol. 24, pp. 373–376, 2006.
31. Wu, W. and Rao, S.S., "Uncertainty analysis and allocation of joint tolerances in robot manipulators based on interval analysis," *Reliability Engineering and System Safety*, Vol. 92, No. 1, pp. 54–64, 2007.
32. Meng, J., Zhang, D.J. and Li, Z.X., "Accuracy Analysis of Parallel Manipulators With Joint Clearance," *ASME Journal of Mechanical Design*, Vol. 131, No. 1, 011013: 1-9, 2009.
33. Drouet, P., Dubowsky, S., Zeghloul, S. and Mavroidis, C., "Compensation of geometric and elastic errors in large manipulators with an application to a high accuracy medical system," *Robotica*, Vol. 20, pp. 341–352, 2007.
34. Gatti, G. and Danieli, G., "Validation of a calibration technique for 6-DOF instrumented spatial linkages," *Journal of Biomechanics*, Vol. 40, pp. 1455–1466, 2002.
35. Briot, S. and Bonev, I.A., "Accuracy analysis of 3-DOF planar parallel robots," *Mechanism and Machine Theory*, Vol. 43, No. 4, pp. 445–458, 2008.
36. Paul, R.P., *Robot manipulators: mathematics, programming, and control*, MIT Press, Cambridge, Massachusetts, 1981.